Free Vibrations of Conical Shells via Ritz Method

R. Vescovini[1]*and N. Fantuzzi[2]

[1] *Dipartimento di Scienze e Tecnologie Aerospaziali, Politecnico di Milano*

Via La Masa 34, 20156 Milano, Italy

[2] *Dipartimento di Ingegneria Civile, Chimica, Ambientale e dei Materiali - Università di Bologna*

Viale del Risorgimento 2, 40136 Bologna, Italy

Abstract

A formulation is presented for investigating the free vibrations of open and closed conical shells. Cylindrical ones are derived as a special case. The approach relies upon an efficient implementation of the Ritz method and allows any set of boundary conditions to be accounted for. In addition, the shells can be stiffened via stringers and/or rings, which are modeled by smearing the properties or by accounting for their discreteness. The resulting models are characterized by relatively few degrees of freedom and reduced computational effort is needed. No meshing is required, so even the modeling phase is conducted quickly. A number of test cases is presented, revealing the accuracy of the proposed strategy and suggesting its use a mean for performing preliminary calculations and assisting the analysis and design process of composite shell structures.

Keywords: Shells; conical shells; cylindrical shells; laminates; stiffened panels; free vibrations.

1 Introduction

Stiffened shells are common structural configurations in several engineering constructions, including aerospace, naval, civil and mechanical ones. They guarantee attractive performance in terms of load carrying capabilities and dynamic response, offering a viable, sometimes more efficient, alternative to an equivalent design based on monolithic architectures. The comparison between stiffened and unstiffened configurations is not trivial [1, 2] and depends on multiple factors to be considered during the design phase, which are inherently multidisciplinary.

Various geometries are commonly used in engineering structures [3], conical and cylindrical ones being the most common ones. Examples are found in the load-carrying structures of space launchers, where both these configurations are commonly used.

Among the structural aspects of interest, the vibratory response plays a crucial role in the design process of shell-like structures. Indeed, this topic is the subject of a vast amount of literature and a comprehensive review

*Corresponding author. *Email address:* `riccardo.vescovini@polimi.it` (Riccardo Vescovini)

is out of the scopes of the present discussion. The interested reader can refer to well-known references [4–9].

Exact solutions are available under specific assumptions on the constitutive law elastic couplings and boundary conditions [7, 8]. For instance, exact solutions are derived for laminated conical shells with orthotropic extension-bending couplings under the assumptions of thin [10] and moderately thick [11] shell theory. Power-series approximation is used in these works and boundary conditions are restricted to simply-supported and clamped edges.

To overcome the difficulties in deriving exact solutions, numerical solution are generally necessary and, for this reason, different strategies have been proposed in the literature. The finite element method (FEM) has received noticeable popularity in the evaluation of shell vibrations, see e.g. [12, 13]. Several formulations in the literature have been developed based on a FEM approach for the assessment of isotropic, composite and FGM shells vibratory response [14–16].

Another well-known approach refers to the Boundary Element Method (BEM). This method has attracted increasing attention in the past years and advanced formulations have been proposed in the literature. For instance, the electroelastic and fracture analysis of ultrathin piezoelectric films/coatings are presented in Refs. [17, 18].

Semi-analytical approaches have also found a large field of employ. Galerkin approaches belong to this class of methods, as well as Ritz-based strategies, the former formulated starting from the governing Partial Differential Equations (PDEs), the latter form an energy standpoint. A loss of generality is somewhat inevitable with respect to FEM. However, this drawback is compensated by reduced time for the analysis and essentially no time for generating the model.

The application of the Ritz method has been a successful approach to derive approximate solutions. Early works in the field refer to isotropic shells. Liew and co-workers developed the pb-2 approach, where shallow shells with single and double curvature are analyzed [19–21]. The extension to thick cylindrical shallow shells is illustrated in Ref. [22] based on a third-order kinematic theory. Free vibrations of conical shells are addressed via mesh-free kp-Ritz method, based on kernel particle, and Love's shell theory in Ref. [23]. A simplified approach is developed in Ref. [24] to analyze the steady-state forced vibrations of isotropic conical shells based on a modal reduction technique, but restricted to simply-supported boundary conditions.

The availability of formulations for laminated conical shells is relatively scarce [25]. Recent works in the literature attempted to handle general boundary conditions in the framework of energy approaches. Interesting examples are found in the Refs. [26–29], where laminated doubly-curved shells of revolution have been studied using penalty terms to enforce virtually any combination of boundary conditions. This strategy is well-known in the literature, see e.g. [30–33], and is appealing owing to its simplicity of implementation. However, the introduction of penalty terms tends to alter the numerical conditioning of the problem and requires some preliminary tuning to define the penalty stiffnesses. Also, the convergence properties of the Ritz method are lost and convergence from above can no more be guaranteed.

The same penalty-based approach is applied to the study of functionally graded [34] and laminated [35] shells. In these works, the displacements are expanded with polynomials and trigonometric functions, although these latter do not form a complete Fourier expansion and may lead to frequency overpredictions. A Gram-Schmidt orthogonalization is proposed in conjunction with a Ritz-like approach for free vibration analysis of conical shells reinforced by functionally graded carbon nanotubes in Ref. [36]. Other approaches have been formulated starting from the strong-form formulation of the problem and referring to the Galerkin method, see e.g. [37, 38] or Differential Quadrature Method (DQM), see [39, 40]. An excellent review on vibrations and stability of conical FGM shells is available in [41].

In the case of stiffened shells, several investigations are found based on a finite element approach [42–47]. In the context of semi-analytical strategies, two main modeling approaches are found in the literature. A first approach relies upon the so-called smearing approach. Main idea is that of averaging the stiffener properties over the shell, thus reducing the analysis of the structure to that of an equivalent monolithic shell. This approach is found in Refs. [48, 49], where exact solutions are derived for free vibrations of smeared cylinders under the assumptions of simply-supported boundary conditions and isotropic [48] and orthotropic materials [49]. More recent applications to stiffened cylinders are found in Refs. [50, 51]. The smeared approach has been applied also to relatively complex shell configurations, including conical shells [52] and joined cylindrical-conical shells with helical stiffeners [53]. An extensive review covering the derivation of smeared properties for many stiffening patterns is found in [54].

The second approach to deal with the presence of stiffening elements consists in modeling them as discrete elements, thus avoiding the process of averaging the contribution onto the shell. Main advantage consists in the possibility of capturing local effects, usually at the expenses of a slightly larger computational cost. The interest for this approach dates back to the early works on isotropic cylindrical [55, 56] and conical shells [57, 58], finding application in more recent works based on the Ritz approach [59, 60]. Restrictions are usually found on boundary conditions that are often taken to be simply-supported [56, 57, 59, 60].

The present work illustrates a highly efficient Ritz-based approach for the free vibration analysis of a wide class of stiffened and unstiffened laminated conical shells within the same unified framework. The approach is developed based on First-order Shear Deformation Theory (FSDT) along with beam models, smeared or discrete, for accounting for the presence of stringers and rings. Conical and cylindrical shells can be studied, either in the form of open panels and closed shells.

This study is motivated by the lack of fast approaches in the literature that are capable of accounting for general shell configurations. Indeed, most semi-analytical strategies refer to simplifying assumptions on boundary conditions and stacking sequences. In the present effort, an approach is proposed to overcome some of the most typical restrictions. In particular, any stacking sequence can be considered – symmetric and unsymmetric, with or without membrane and flexural anisotropy – as well as any combination of in-plane and out-of-plane constraints is accounted for. In addition, the possibility of considering conical shells with longitudinal and transverse stiffeners renders the approach very general, in contrast with the vast majority of works in the literature which are developed for a specific class of structures. The computational effectiveness of the approach is guaranteed by the analytical integration of the Ritz integrals, an approach firstly proposed by the first author in a recent effort for plate analysis [61], but still not applied to the case of conical stiffened shells.

The work is organized as follows: Section 2 provides an overview of the formulation, illustrating the kinematic assumptions and the energy formulation; Section 3 discusses the approximate solution strategy via Ritz method with focus on its effective implementation; Section 4 provides a set of test cases to validate the method against reference results and illustrate the effectiveness of the approach; conclusions and future developments are discussed in Section 5.

2 Formulation

This study presents a formulation for the analysis of stiffened and unstiffened shells. These structures can be in the form of closed shells or open panels. For generality, conical geometry is considered below. The special case of circular cylindrical curvature can be recovered as a special case.

A sketch of the structure under investigation is reported in Figure 1, where the relevant dimensions are indicated. Specifically, the shell is characterized by length a, semi-vertex angle α, radii at the two ends R_i and R_e and thickness h. The opening angle is denoted with θ.

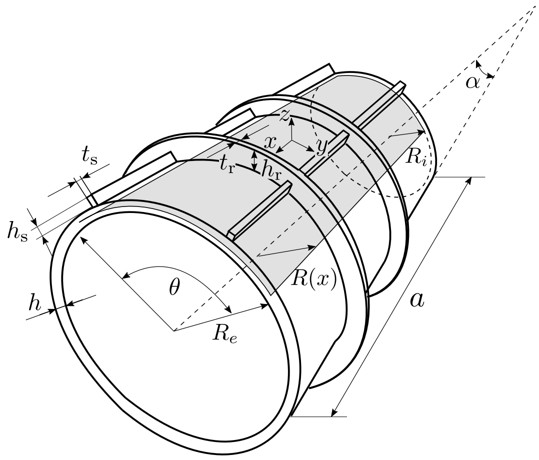

Figure 1: Shell geometry and dimensions.

Both isotropic and composite materials are considered. In this second case, the shell is obtained by the stacking of a number of plies with orthotropic properties, each characterized by a specific orientation angle, under the assumption that they are perfectly bonded at each other. Within the same framework, FGM materials can be considered too.

The shell can be stiffened along the meridional and circumferential direction by N_{s} stringers and N_{r} rings. For the stringers, the height and the width are denoted with h_s and t_s, respectively. For the rings the same notation applies upon replacement of the subscript s with r.

The eccentricities of stringers and rings are denoted with e_s and e_r and represent the distance of the elastic centroid of the section measured from the skin midsurface. Positive values imply external stiffening, while negative values are associated with internal stiffening elements.

The formulation relies on First-Order Shear Deformation Theory (FSDT) to model the skin of the panel, so that transverse shear deformation effects can be accounted for and moderately thick configurations can be studied. Stringers and rings are modeled as beam elements as, in typical applications, they are characterized by one direction which is much larger with respect to the other two. In doing so, local effects and section deformability cannot be accounted for, but these effects are not of interest within the range of low/middle frequencies. Consistently with the shell kinematics, also beam elements account for transverse shear deformation via first-order theory. An analogous approach relying con Classical Lamination Theory (CLT) has been developed within the framework illustrated next, but is not reported here for the sake of brevity.

The reference surface of the shell is identified in correspondence of the midplane, and a curvilinear reference system is taken with the x and y axes running in the meridional and circumferential direction. The z direction is taken positive to obtain a right-handed reference system, thus pointing toward the outer direction.

The origin of the system is in the middle of the shell, such that the top/bottom edges are located at $x = \mp a/2$ and, in the case of panels, the lateral edges are at $y = \mp \frac{R\theta}{2}$, where the horizontal radius of a generic shell parallel is obtained as:

$$R(x) = R_i + x \sin\alpha \tag{1}$$

2.1 Kinematics

In the framework of FSDT, the displacement field is represented as:

$$u(x,y,z) = u_0(x,y) + z\varphi_x(x,y), \quad v(x,y,z) = v_0(x,y) + z\varphi_y(x,y), \quad w(x,y,z) = w_0(x,y) \tag{2}$$

where $\mathbf{u} = \{u_0, v_0, w_0, \varphi_x, \varphi_y\}^\mathrm{T}$ is the vector of the generalized displacement components of the kinematic model. The expression of Eq. (2) is meant as a kinematic rule to allow the displacement of a generic point of coordinates (x, y, z) to be represented by considering a corresponding point belonging to the reference surface.

The strain-displacement relations for membrane deformations for a conical shell are given as [8, 39]:

$$\varepsilon_x^0 = u_{0,x}, \quad \varepsilon_y^0 = v_{0,y} + \frac{u_0}{R}\sin\alpha + \frac{w_0}{R}\cos\alpha, \quad \gamma_{xy}^0 = u_{0,y} + v_{0,x} - \frac{v_0}{R}\sin\alpha \tag{3}$$

where comma is used to denote the derivative with respect to a direction. Accordingly, the curvatures are obtained through the relations:

$$k_{xx} = \varphi_{x,x}, \quad k_{yy} = \varphi_{y,y} + \frac{\varphi_x}{R}\sin\alpha, \quad k_{xy} = \varphi_{y,x} \quad k_{yx} = \varphi_{x,y} - \frac{\varphi_y}{R}\sin\alpha \tag{4}$$

the first two terms representing the bending-related curvatures, the last one describing the twisting deformation. In the context of FSDT, transverse shear strains are accounted for, and their expression reads:

$$\gamma_{zy}^0 = w_{0,y} - \frac{v_0}{R}\cos\alpha + \varphi_y, \quad \gamma_{zx}^0 = w_{0,x} + \varphi_x \tag{5}$$

In view of future developments, the generalized strain parameters are conveniently collected into three vectors, i.e:

$$\boldsymbol{\varepsilon}^0 = \{\varepsilon_x^0 \quad \varepsilon_y^0 \quad \gamma_{xy}^0\}^{\mathrm{T}}, \quad \mathbf{k} = \{k_{xx} \quad k_{yy} \quad \tau = k_{xy} + k_{yx}\}^{\mathrm{T}}, \quad \boldsymbol{\gamma} = \{\gamma_{zy}^0 \quad \gamma_{zx}^0\}^{\mathrm{T}} \tag{6}$$

The three vectors of Eq. (6) define the membrane strains, the curvatures and the shearing deformations.

The boundary conditions are specified by means of a short notation where each letter defines the constraints at each edge of the shell. For open panels, four letters are used, denoting the edges at $x = -a/2$, $y = -\frac{R\theta}{2}$, $x = a/2$ and $y = \frac{R\theta}{2}$. For closed shells, two letters are used to denote the boundary conditions at the top and the bottom of the structure at $x = \mp a/2$. Any set of boundary conditions can be accounted for within the proposed framework. For the scopes of this paper, four conditions are considered, namely clamped (C), simply-supported 1 (S), simply-supported 2 (s) and free (F). In particular, the corresponding essential boundary conditions are:

Clamped – C

$$\begin{aligned} &u_0 = v_0 = w_0 = \varphi_x = \varphi_y = 0 \ \text{ at } x = \mp a/2 \\ &u_0 = v_0 = w_0 = \varphi_x = \varphi_y = 0 \ \text{ at } y = \mp\frac{R\theta}{2} \end{aligned} \tag{7}$$

Simply-supported (movable) – S

$$\begin{aligned} &v_0 = w_0 = \varphi_y = 0 \ \text{ at } x = \mp a/2 \\ &u_0 = w_0 = \varphi_x = 0 \ \text{ at } y = \mp\frac{R\theta}{2} \end{aligned} \tag{8}$$

Simply-supported (immovable) – s

$$\begin{aligned} &u_0 = v_0 = w_0 = \varphi_y = 0 \ \text{ at } x = \mp a/2 \\ &u_0 = v_0 = w_0 = \varphi_x = 0 \ \text{ at } y = \mp\frac{R\theta}{2} \end{aligned} \tag{9}$$

Note, the natural boundary conditions are not reported here as they are fulfilled in a weak-form sense owing to the variational approach developed in this work. The case of free edge (F) does not involve any essential boundary condition, so it is not reported above.

2.2 Weak-form

The approach is developed by referring to the weak-form formulation of the problem, which is particularly suitable for the numerical approximation. The Hamilton's principle is used for this scope. In particular, the variational principle for an elastic continuum body states that [62]:

$$\delta \int_{t_1}^{t_2} (K - U)\,\mathrm{d}t = 0 \tag{10}$$

where K is the kinetic energy and U the strain energy stored in the body. For the stiffened structures under investigation, it is useful to decompose these terms as:

$$U = U_{\text{sh}} + U_{\text{s}} + U_{\text{r}}, \qquad K = K_{\text{sh}} + K_{\text{s}} + K_{\text{r}} \tag{11}$$

where the subscripts sh, s and r identify the contributions arising from the shell, the stringers and the stiffeners. For a shell modeled via FSDT, the strain energy is obtained as:

$$U_{\text{sh}} = \frac{1}{2}\int_S \left(\begin{Bmatrix} \boldsymbol{\varepsilon}^0 \\ \mathbf{k} \end{Bmatrix}^{\text{T}} \begin{bmatrix} \mathbf{A} & \mathbf{B} \\ \mathbf{B} & \mathbf{D} \end{bmatrix} \begin{Bmatrix} \boldsymbol{\varepsilon}^0 \\ \mathbf{k} \end{Bmatrix} + \boldsymbol{\gamma}^{\text{T}} \mathbf{A}^{\text{s}} \boldsymbol{\gamma} \right) \mathrm{d}x\,\mathrm{d}y \tag{12}$$

where $\mathbf{A}$, $\mathbf{B}$, $\mathbf{D}$ and $\mathbf{A}^{\text{s}}$ define the shell constitutive law and represent the membrane, coupling, bending and transverse shear stiffnesses.

The shell kinetic energy is:

$$K_{\text{sh}} = \frac{1}{2}\int_S \dot{\mathbf{u}}^{\text{T}} \mathbf{M}_{\text{sh}} \dot{\mathbf{u}}\,\mathrm{d}x\,\mathrm{d}y = \frac{1}{2}\int_S \begin{Bmatrix} \dot{u}_0 \\ \dot{v}_0 \\ \dot{w}_0 \\ \dot{\varphi}_x \\ \dot{\varphi}_y \end{Bmatrix}^{\text{T}} \begin{bmatrix} I_0 & 0 & 0 & I_1 & 0 \\ 0 & I_0 & 0 & 0 & I_1 \\ 0 & 0 & I_0 & 0 & 0 \\ I_1 & 0 & 0 & I_2 & 0 \\ 0 & I_1 & 0 & 0 & I_2 \end{bmatrix} \begin{Bmatrix} \dot{u}_0 \\ \dot{v}_0 \\ \dot{w}_0 \\ \dot{\varphi}_x \\ \dot{\varphi}_y \end{Bmatrix} \mathrm{d}x\,\mathrm{d}y \tag{13}$$

where $\mathbf{M}_{\text{sh}}$ is the shell mass matrix and the entries I_i are defined as:

$$\{I_0, I_1, I_2\} = \int_h \rho\{1, z, z^2\}\,\mathrm{d}z \tag{14}$$

The contributions of stringers and rings have different expressions depending on whether they are modeled as discrete elements or smeared onto the skin surface. In the first case, their contribution can be expressed as:

$$\{U_{\text{s}}, K_{\text{s}}\} = \sum_{i=1}^{N_{\text{s}}} \int_0^a \{\mathcal{U}_{\text{s}}, \mathcal{K}_{\text{s}}\}\mathrm{d}x \Bigg|_{y=y_i}, \qquad \{U_{\text{r}}, K_{\text{r}}\} = \sum_{i=1}^{N_{\text{r}}} \int_0^{\theta R} \{\mathcal{U}_{\text{r}}, \mathcal{K}_{\text{r}}\}\mathrm{d}y \Bigg|_{x=x_i} \tag{15}$$

where $\mathcal{U}$ and $\mathcal{K}$ denote the strain and kinetic energy densities. A line integral is carried out along the beam axis for each stiffening element. Discreteness is accounted for by evaluation of the relevant quantities appearing in Eq. (15) in correspondence of the coordinate x_i or y_i of the beam element.

The energy densities associated with the stringers are easily obtained by combining first-order beam kinematics and enforcing the compatibility between the beam and the shell displacements. This leads to:

$$\mathcal{U}_{\text{s}} = \frac{1}{2} \begin{Bmatrix} \varepsilon_x^0 \\ k_{xx} \end{Bmatrix}^{\text{T}} \mathbf{C}_{\text{s}} \begin{Bmatrix} \varepsilon_x^0 \\ k_{xx} \end{Bmatrix} + \frac{1}{2}\left(GJ_{\text{s}} k_{xy}^2 + GA_{\text{s}} {\gamma_{zx}^0}^2 \right), \qquad \mathcal{K}_{\text{s}} = \frac{1}{2} \begin{Bmatrix} \dot{u}_0 \\ \dot{w}_0 \\ \dot{\varphi}_x \end{Bmatrix}^{\text{T}} \mathbf{M}_{\text{s}} \begin{Bmatrix} \dot{u}_0 \\ \dot{w}_0 \\ \dot{\varphi}_x \end{Bmatrix} \tag{16}$$

where GJ_s and GA_s are the torsional and shearing stiffnesses, while the stiffness and mass matrices $\mathbf{C}_\mathrm{s}$ and $\mathbf{M}_\mathrm{s}$ are defined as:

$$\mathbf{C}_\mathrm{s} = \begin{bmatrix} EA_\mathrm{s} & e_\mathrm{s}EA_\mathrm{s} \\ e_\mathrm{s}EA_\mathrm{s} & EJ_\mathrm{s} + EA_\mathrm{s}e_\mathrm{s}^2 \end{bmatrix}, \qquad \mathbf{M}_\mathrm{s} = \rho \begin{bmatrix} A_\mathrm{s} & 0 & A_\mathrm{s}e_\mathrm{s} \\ 0 & A & 0 \\ A_\mathrm{s}e_\mathrm{s} & 0 & J_\mathrm{s} + A_\mathrm{s}e_\mathrm{s}^2 \end{bmatrix} \tag{17}$$

From the expressions of Eq. (17), one can note that eccentricity promotes a coupling effect between in-plane and out-of-plane response, as seen by the off-diagonal terms. The energy contributions of Eq. (16) neglect the effect of in-plane rotatory inertia. These contributions are responsible for more complex resulting equations, while providing negligible improvements to the numerical predictions. Their effect has been studied within the present formulation and it is then believed advantageous to neglect these terms.

In a similar fashion, the contribution due to the circumferential stiffening elements is obtained as:

$$\mathcal{U}_\mathrm{r} = \frac{1}{2}\begin{Bmatrix} \varepsilon_y^0 \\ k_{yy} \end{Bmatrix}^\mathrm{T} \mathbf{C}_\mathrm{r} \begin{Bmatrix} \varepsilon_y^0 \\ k_{yy} \end{Bmatrix} + \frac{1}{2}\left(GJ_\mathrm{r}k_{yx}^2 + GA_\mathrm{r}{\gamma_{zy}^0}^2\right), \qquad \mathcal{K}_\mathrm{r} = \frac{1}{2}\begin{Bmatrix} \dot{v} \\ \dot{w} \\ \dot{\varphi}_y \end{Bmatrix}^\mathrm{T} \mathbf{M}_\mathrm{r} \begin{Bmatrix} \dot{v} \\ \dot{w} \\ \dot{\varphi}_y \end{Bmatrix} \tag{18}$$

where the stiffness and mass matrices $\mathbf{C}_\mathrm{r}$ and $\mathbf{M}_\mathrm{r}$ have the expression reported in Eq. (17) by replacing stiffener-related quantities with ring ones.

A second modeling approach for stringers and rings relies upon the so-called smearing-technique. The rationale behind this strategy consists in replacing these elements with equivalent layers of material to be added to the skin. In doing so, the stiffened shell is studied as an equivalent unstiffened shell, modified through the addition of extra layers of material. Historically, this approach has been widely employed for two main reasons. Firstly, it allows simple analytical solutions to be derived, which are useful for preliminary design scopes. This is especially true for cylindrical shells and flat plates, see [48]. Secondly, it furnishes a physically-grounded approach for developing finite element models based on shell elements only, thus avoiding the need for computationally expensive models when stiffeners or rings are relatively close to each other.

In the context of the Ritz-based formulation developed here, the advantages offered by a smeared approach are milder, as the absence of a computational grid renders the modeling of the structure essentially independent on the number of stiffeners and rings. However, it is of interest to extend the approach to the case of smeared stiffening elements in order to gather insight into the modeling issues associated with this approach.

The energy contributions of the smeared stiffeners/rings are simply obtained by averaging their contribution over the skin of the panel, i.e.:

$$\begin{aligned} \{U_\mathrm{s}, K_\mathrm{s}\} &= \frac{N_\mathrm{s}}{\theta}\int_S \frac{1}{R}\{\mathcal{U}_\mathrm{s}, \mathcal{K}_\mathrm{s}\}\mathrm{d}x\mathrm{d}y \\ \{U_\mathrm{r}, K_\mathrm{r}\} &= \frac{N_\mathrm{r}}{a}\int_S \{\mathcal{U}_\mathrm{r}, \mathcal{K}_\mathrm{r}\}\mathrm{d}x\mathrm{d}y \end{aligned} \tag{19}$$

where the energy densities are those reported in Eqs. (16) and (18). Owing to the smeared approach, the beam energy contributions of Eq. (19) are converted back to surface integrals, which are then handled similarly to the skin-related ones.

3 Ritz method

The stationary condition implied by Eq. (10) is imposed after approximating the generalized displacements using global functions. With this purpose in mind, it is useful to first introduce a computational domain by the transformation:

$$\xi = \frac{2}{a}x, \quad \eta = \frac{2}{\theta R}y \tag{20}$$

with the natural coordinates $\eta, \xi \in [-1\,1]$. Accordingly, all the surface integrals expressing the energy contributions can be transformed as:

$$\int_S (\cdot)\, \mathrm{d}x\, \mathrm{d}y = \int_{-1}^{+1} \int_{-1}^{+1} (\cdot)\, \frac{\theta R}{2} \frac{a}{2}\, \mathrm{d}\xi\, \mathrm{d}\eta \tag{21}$$

which a suitable form to perform the integrals required by the Ritz approximation, either numerically and analytically. The approximation of the problem consists in expanding the unknowns, i.e. the generalized displacement components, using a summatory of appropriately chosen trial functions. It is assumed that separation of variables can be operated, so:

$$\begin{aligned} u_\alpha(\xi,\eta) &= \sum_{mn}^{M_\alpha N_\alpha} q_{u_\alpha mn} \varphi_{u_\alpha\, m}(\xi) \psi_{u_\alpha n}(\eta) = \\ &= \left(\boldsymbol{\varphi}_{u_\alpha}^{\mathrm{T}} \otimes \boldsymbol{\psi}_{u_\alpha}^{\mathrm{T}}\right) \mathbf{q}_{u_\alpha} \qquad u_\alpha \in \{u_0,\ v_0,\ w_0,\ \varphi_x,\ \varphi_y\} \end{aligned} \tag{22}$$

where M_α and N_α denote the number of functions to expand the generic displacement component u_α along the directions ξ and η, respectively; the vectors appearing in Eq. (22) are defined as $\boldsymbol{\varphi}_{u_\alpha} = \{\varphi_{u_\alpha\,1},\ \ldots,\ \varphi_{u_\alpha\, M_\alpha}\}^{\mathrm{T}}$ and $\boldsymbol{\psi}_{u_\alpha} = \{\psi_{u_\alpha\,1},\ \ldots,\ \psi_{u_\alpha\, N_\alpha}\}^{\mathrm{T}}$, where each entry of the two vectors is a function that identically satisfies the essential conditions of the problem; these functions are also part of a complete series and do satisfy complementary conditions [63]. Consistently with this sorting of the trial functions, the vector collecting the unknown amplitudes is defined as $\mathbf{q}_{u_\alpha} = \{q_{u_\alpha 11},\ q_{u_\alpha 12},\ \ldots,\ q_{u_\alpha M_\alpha N_\alpha}\}^{\mathrm{T}}$.

Based on the change of coordinates of Eq. (20), the spatial derivatives of Eq. (22) are computed as:

$$u_{\alpha,x} = \left(\boldsymbol{\varphi}_{u_\alpha}^{(1)^{\mathrm{T}}} \otimes \boldsymbol{\psi}_{u_\alpha}^{\mathrm{T}}\right) \frac{2}{a}, \quad u_{\alpha,y} = \left(\boldsymbol{\varphi}_{u_\alpha}^{\mathrm{T}} \otimes \boldsymbol{\psi}_{u_\alpha}^{(1)^{\mathrm{T}}}\right) \frac{2}{\theta R} \tag{23}$$

where use is made of the following compact notation to denote the derivatives with respect to the natural coordinates:

$$(\cdot)^{(i)} = \frac{\partial\,(\cdot)}{\partial \xi^i}, \qquad (\cdot)^{(j)} = \frac{\partial\,(\cdot)}{\partial \eta^j} \tag{24}$$

3.1 Trial functions

The choice of trial functions is a crucial step in a Ritz-based procedure. Indeed, different sets of functions are known to affect the solution of the problem in terms of accuracy, stability, sparsity of the resultant matrices and, ultimately, in computational time [61].

A distinction is made between the case of open and closed shells. In the first case, the trial functions are defined on the basis of the boundary conditions at the four edges. In the second case, the functions are required to satisfy the essential conditions at the top and the bottom, while satisfying the continuity condition along the circumferential direction (periodicity condition).

For open shells, i.e. panels, the displacements are expanded as:

$$\varphi_{u_\alpha\, m}(\xi) = b^{\xi}_{u_\alpha}(\xi) P_m(\xi), \qquad \psi_{u_\alpha\, n}(\eta) = b^{\eta}_{u_\alpha}(\eta) P_n(\eta) \tag{25}$$

where the notation P_i is introduced to denote the Legendre polynomial of order i, whilst $b^{\xi}_{u_\alpha}$ and $b^{\eta}_{u_\alpha}$ are the boundary functions introduced to enforce the essential conditions of the component u_α at the edges at $\xi = \pm 1$ and $\eta = \pm 1$, respectively. It is worth noting that any complete expansion could be used to replace Legendre polynomials in Eq. (25). Examples are given by Jacobi or Chebyshev polynomials. All these solutions proved to be less effective with respect to Legendre polynomials, as they are responsible for a less pronounced degree of sparsity in the resulting stiffness matrices [61].

For closed shells, the proposed approach relies upon a combination of polynomial and trigonometric functions. In particular, the expansion along the meridional direction remains unchanged, so:

$$\varphi_{u_\alpha\, m}(\xi) = b_{u_\alpha}(\xi) P_m(\xi) \tag{26}$$

whereas the expansion in the circumferential direction is modified in order to impose continuity of displacements and rotations at $\eta = \pm 1$. Trigonometric functions are used for this scope, i.e.:

$$\psi_{u_\alpha\, 0} = 1; \quad \psi_{u_\alpha\, n} = \cos \frac{n\pi(\eta + 1)}{2} \quad (n \text{ odd}); \quad \psi_{u_\alpha\, n} = \sin \frac{n\pi(\eta + 1)}{2} \quad (n \text{ even}) \tag{27}$$

It is worth noting that the approximation operated along the direction η requires all the terms of a complete Fourier expansion, including the constant contribution. The circumferential approximation is often overlooked in the literature and it is not uncommon to find formulations restricted on the use of sine terms, only: this strategy stems from the Navier solution available under specific restrictions on boundary conditions and stacking sequences, but cannot be applied to study general laminates and constraints.

The number of the trial functions for the analysis is typically chosen based on preliminary convergence studies. The use of approximately 20 functions along both directions guarantees adequate spatial resolution in most cases, but each single problem has to be studied individually based on its specific features, such as mode localizations or complicating effects due to anisotropy. By increasing the terms retained in the expansion, the accuracy of the predictions can be progressively increased. Note that increasing the number of terms does not imply the whole evaluation of the stiffness and mass matrices: only the new terms need to be computed. One side effect of increasing the number of trial functions regards the worsening of the conditioning number of the stiffness matrix – this consideration holds true for polynomials functions, for trigonometric ones this problem is inherently overcome. However, previous studies [61] proved the numerical robustness of the orthogonal polynomials, which can be successfully employed up to expansions of hundreds of terms along each single direction with no ill-conditioning issues.

3.2 Ritz integrals

The Ritz method allows the continuum problem to be transformed into a discrete one upon replacement of Eq. (22) into the relevant variational principle. This operation leads to the need for evaluating surface integrals, which is often a bottle-neck in the development of Ritz-based approaches. An effective approach for overcoming this obstacle is discussed below, where the approach for evaluating the Ritz integrals is outlined. Owing to the separation of variables operated in Eq. (22), the surface integrals can be conveniently split into the product of two line integrals as:

$$\int_{-1}^{+1}\int_{-1}^{+1}(\cdot)\,\mathrm{d}\xi\,\mathrm{d}\eta=\int_{-1}^{+1}(\cdot)\,\mathrm{d}\xi\int_{-1}^{+1}(\cdot)\,\mathrm{d}\eta \tag{28}$$

The contribution associated with the integration along the meridional direction ξ can be generically written as:

$$^{h}\mathbf{I}^{df}_{u_\alpha u_\beta}=\int_{-1}^{+1}R^h\boldsymbol{\varphi}^{(d)^{\mathrm{T}}}_{u_\alpha}\otimes\boldsymbol{\varphi}^{(f)}_{u_\beta}\,\mathrm{d}\xi\qquad h\in\{-1,\ 0,\ 1,\ 2\} \tag{29}$$

where $R=R(\xi)=a/2\,(1+\xi)\sin\alpha+R_i$; the indexes d and f denote the order of the derivatives of the trial functions, while h is the exponent of the radius. When $h=0$, the integrals can be evaluated analytically. On the contrary, when the integrand function depends on the radius $R=R(\xi)$, then a Gauss-based numerical integration is sought as:

$$^{h}\mathbf{I}^{df}_{u_\alpha u_\beta}\approx\sum_{i=1}^{N_{\mathrm{ip}}}w_iR^h(\xi_i)\boldsymbol{\varphi}^{(d)^{\mathrm{T}}}_{u_\alpha}(\xi_i)\otimes\boldsymbol{\varphi}^{(f)}_{u_\beta}(\xi_i) \tag{30}$$

where N_{ip} is the number of integration points, ξ_i and w_i the coordinates and the weights of the integration points.

Accordingly the integration along the circumferential direction is carried out as:

$$\mathbf{J}^{eg}_{u_\alpha u_\beta}=\int_{-1}^{+1}\boldsymbol{\psi}^{(e)^{\mathrm{T}}}_{u_\alpha}\otimes\boldsymbol{\psi}^{(g)}_{u_\beta}\,\mathrm{d}\eta \tag{31}$$

Here the indexes e and g are introduced to specify the order of the derivatives of the trial funcitons. Note, the integrals above are independent on the radius of curvature, so they can be evaluated analytically just once.

The evaluation of the energy contributions associated with discrete stringers and rings implies the need for evaluating the trial functions in correspondence of the beam position, see Eq. (15). Each stringer is associated with a known position η_i defining its position along the circumferential direction. Similarly, the rings are defined by ξ_i. The trial functions are then organized as:

$$_{i}\mathcal{I}^{df}_{u_\alpha u_\beta}=\boldsymbol{\varphi}^{(d)^{\mathrm{T}}}_{u_\alpha}(\xi_i)\otimes\boldsymbol{\varphi}^{(f)}_{u_\beta}(\xi_i) \tag{32}$$

$$_{j}\mathcal{J}^{eg}_{u_\alpha u_\beta}=\boldsymbol{\psi}^{(e)^{\mathrm{T}}}_{u_\alpha}(\eta_j)\otimes\boldsymbol{\psi}^{(g)}_{u_\beta}(\eta_j) \tag{33}$$

which are nothing but matrices collecting the evaluation of the functions in specific locations. These terms cannot be computed a-priori as they are dependent on the position of rings and stringers, which are data of the problem. However, the evaluation of these terms is straightforward and can be carried out in fractions of a second.

3.3 Discrete problem

The Ritz approximation of the unknown displacement field leads to a discrete problem in the form of a standard eigenvalue problem. In particular, the strain energy stored in the shell is obtained upon substitution of Eq. (22) into Eq. (11) and is represented as:

$$U = \frac{1}{2} \sum_{u_\alpha u_\beta} \mathbf{q}_{u_\alpha}^{\mathrm{T}} \mathbf{K}_{u_\alpha u_\beta} \mathbf{q}_{u_\beta} \tag{34}$$

Similarly, the kinetic energy arising from the shell harmonic motion reads:

$$K = \frac{\omega^2}{2} \sum_{u_\alpha u_\beta} \mathbf{q}_{u_\alpha}^{\mathrm{T}} \mathbf{M}_{u_\alpha u_\beta} \mathbf{q}_{u_\beta} \tag{35}$$

where the blocks $\mathbf{K}_{u_\alpha u_\beta}$ and $\mathbf{M}_{u_\alpha u_\beta}$ are assembled to obtain the final stiffness and mass matrix of the problem and leading to the standard eigenvalue problem to be solved in the form:

$$\left(-\omega^2 \mathbf{M} + \mathbf{K}\right) \mathbf{q} = \mathbf{0} \tag{36}$$

The expressions for the blocks composing the final matrices is outlined below for the stiffness terms only: the handling of the mass matrix is conducted with a similar approach. In particular, the stiffness matrix block appearing in Eq. (34) is available as the sum of the skin, stringer and rings contributions as:

$$\mathbf{K}_{u_\alpha u_\beta} = \frac{\partial^2 U}{\partial \mathbf{q}_{u_\alpha} \partial \mathbf{q}_{u_\beta}} = \frac{\partial^2 \left(U_{\mathrm{sh}} + U_{\mathrm{s}} + U_{\mathrm{r}}\right)}{\partial \mathbf{q}_{u_\alpha} \partial \mathbf{q}_{u_\beta}} = \mathbf{K}_{u_\alpha u_\beta}^{\mathrm{sh}} + \mathbf{K}_{u_\alpha u_\beta}^{\mathrm{s}} + \mathbf{K}_{u_\alpha u_\beta}^{\mathrm{r}} \tag{37}$$

and the the skin-related term $\mathbf{K}_{u_\alpha u_\beta}^{\mathrm{sh}}$ can be generically expressed as:

$$\mathbf{K}_{u_\alpha u_\beta}^{\mathrm{sh}} = \sum_{defgh} {}^{h}\mathbf{I}_{u_\alpha u_\beta}^{df} \otimes \mathbf{J}_{u_\alpha u_\beta}^{eg} E_{defgh}^{\mathrm{sh}} \tag{38}$$

where a Kronecker product is conducted between the Ritz integrals of Eqs. (29) and (31), which requires reduced computational effort. The coefficients E_{defgh}^{sh} collect the dependency on the laminate elastic properties and the shell geometry. The expression of these terms is relatively lengthy and is not reported here for the sake of brevity.

The contributions due to stringers and rings need to be distinguished between the case of discrete and smeared modeling. In the first case, the corresponding contributions are obtained in the form:

$$\mathbf{K}_{u_\alpha u_\beta}^{\mathrm{s}} = \sum_{i=1}^{\mathrm{N_s}} \sum_{defgh} {}^{h}\mathbf{I}_{u_\alpha u_\beta}^{df} \otimes {}_{i}\mathcal{J}_{u_\alpha u_\beta}^{eg} E_{defgh}^{\mathrm{s}} \tag{39}$$

$$\mathbf{K}_{u_\alpha u_\beta}^{\mathrm{r}} = \sum_{j=1}^{\mathrm{N_r}} \sum_{defgh} {}_{i}\mathcal{I}_{u_\alpha u_\beta}^{df} \otimes \mathbf{J}_{u_\alpha u_\beta}^{eg} E_{defgh}^{\mathrm{r}} \tag{40}$$

where the trial functions are integrated along one direction only and are evaluated in correspondence of structural element on the other, according to Eqs. (32) and (33).

In case of smeared stringers and rings, the averaging process implied by Eq. (19) leads to stiffness terms in the form:

$$\mathbf{K}^{\mathrm{s}}_{u_\alpha u_\beta} = \sum_{defgh} {}^{h}\mathbf{I}^{df}_{u_\alpha u_\beta} \otimes \mathbf{J}^{eg}_{u_\alpha u_\beta} \hat{E}^{\mathrm{s}}_{defgh} \tag{41}$$

$$\mathbf{K}^{\mathrm{r}}_{u_\alpha u_\beta} = \sum_{defgh} {}^{h}\mathbf{I}^{df}_{u_\alpha u_\beta} \otimes \mathbf{J}^{eg}_{u_\alpha u_\beta} \hat{E}^{\mathrm{r}}_{defgh} \tag{42}$$

which are formally analogous to the skin-related contribution of Eq. (38). By inspection of Eqs. (41) and (42), one can observe a simplification with respect Eqs. (39) and (40) – these latter relative to the discrete modeling of rings and stiffeners –, as no summatory is required over the one structural elements. This feature can be of advantage in the presence of configurations characterized by several stringers and/or rings. Clearly, one can combine discrete stringers with smeared rings and viceversa depending on the modeling needs.

4 Results

This section is devoted to presenting a number of test cases including different class of structures, ranging from cylindrical to conical shells, closed and open, with or without stiffening elements and made of isotropic and anisotropic materials. Indeed, the formulation developed here offers a wide range of applicability and can be successfully applied to perform preliminary studies on various sets of design.

In addition to showcase the potential application to various design scenarios, this section aims at presenting the high efficiency of the code by reporting the results obtained using a relatively high number of trial functions. As compared to most of the works in the literature, the evaluation of the integrals is conducted analytically, whenever possible. Thus, governing equations can be derived on the fly and enlarged basis of trial functions can be easily handled. This advantage is exploited for reporting reference results.

The importance of adopting appropriate sets of functions is discussed with reference to anisotropic configurations, where erroneous results can sometimes be obtained if proper care is not provided. In addition, the analysis of stiffened configurations is conducted by illustrating the advantage of adopting a discrete stiffener modeling against a smeared one.

All the computations reported in this section are conducted by considering a shear factor equal to 5/6. In-plane and rotational inertia are accounted for and the number of trial functions is taken equal to R=S=20, unless otherwise stated. This choice stems from the preliminary convergence studies reported at the beginning of the next section, illustrating this expansion to be adequate in most cases. The Ritz functions considered next are those of Eqs. (25)-(27). When a Navier-type approach is adopted, this is explicitly stated.

4.1 Unstiffened shells

Example 1: isotropic cylindrical and conical shells

Goal of this first example is illustrating the effectiveness of the method in analyzing both cylindrical and conical shells, providing some insights on the convergence of the method. Open and closed-shell configurations are studied for this purpose. In addition, the results reported herein aim at providing evidence of the capability of the proposed implementation in representing a wide set of constraints, other than the simply-supported ones usually considered in many semi-analytical approaches.

The test case is taken from Ref. [39], where moderately thick shells are analyzed using the GDQ method and FSDT theory. Specifically, cylindrical and conical panels are considered, as well as closed cylinders and cones. All the structures have length 2000 mm and thickness 100 mm. The panels, both for cylindrical and conical curvatures, present an opening angle equal to θ=120°; conical shells – open and closed – have radius R_i=500 mm and semi-vertex angle α=40°. The material is isotropic and is characterized by the following properties: E=210 GPa, ν=0.3 and ρ=7.8×10^{-9} t/mm^3.

As a first step, the convergence of the method is assessed. This preliminary study allows to gather insight into the number of functions to be used in the analysis. In particular, the plots of Figures 2 and 3 report the results for cylindrical and conical shells, respectively, subjected to different sets of boundary conditions: FFCF and FFss for panels, and FC and ss for closed shells. The presence of free edges is believed of particular interest as the corresponding boundary conditions are not satisfied a priori, but they are fulfilled in a weak-form sense during the convergence of the solution. The curves report the number of trial functions against the percent error in logarithmic scale for the first four frequencies. As no exact solutions are available, the error is computed against the solution obtained with 50×50 functions.

The results clearly illustrate the faster convergence in the case of closed shells, i.e. cylinders and cones, – the percent error drops to very small values with relatively few functions. By inspection of the results of Figures 2 and 3, it is noted that, for a fixed number of functions, smaller errors are achieved in case of cylindrical curvature. The differences ascribable to the boundary conditions are relatively small. To define the number of trial functions, one possible approach consists in defining a threshold in terms of percent error with respect to the reference solution. For the problem at hand, a threshold equal to 0.01% leads to R=S=20.

The second part of the section aims at illustrating the accuracy of the method by comparison against reference results and Abaqus calculations. The finite element models are based on S4R elements with a mesh density chosen on the basis of a preliminary convergence study, with a typical element size equal to 50 mm. A summary of the results is reported in Table 1 for the case of open shells. The first eight dimensional frequencies are reported for a number of Ritz functions R=S guaranteeing convergence up to the last digit reported. One can observe that slightly more than 20 functions are needed in all cases.

The results are in excellent agreement with the ones of Ref. [39] where a different numerical strategy is

NEW FIGURE

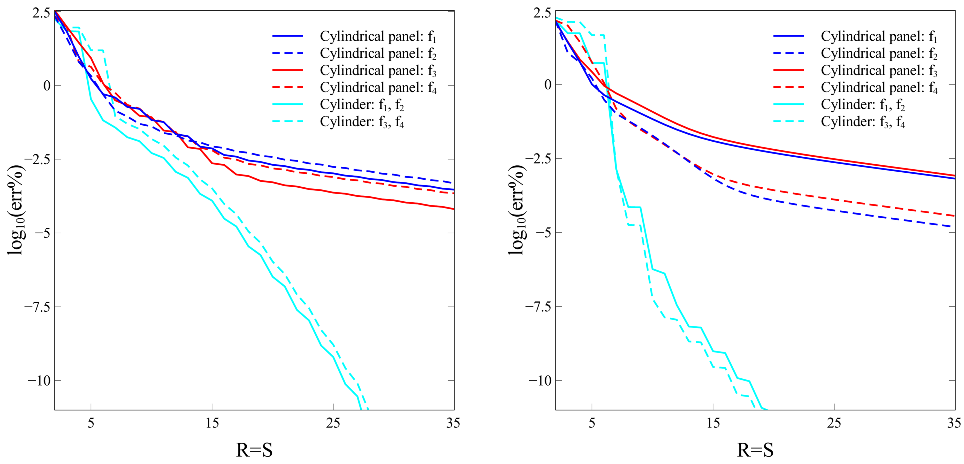

(a) (b)

Figure 2: Logarithmic error versus number of trial functions R=S for the first 4 frequencies for isotropic cylindrical shells (a=2000 mm, R_i=1000 mm, h=100 mm) with different boundary conditions: (a) FFCF (panels, θ=120°), FC (cylinders), (b) FFss (panels, θ=120°), ss (cylinders).

NEW FIGURE

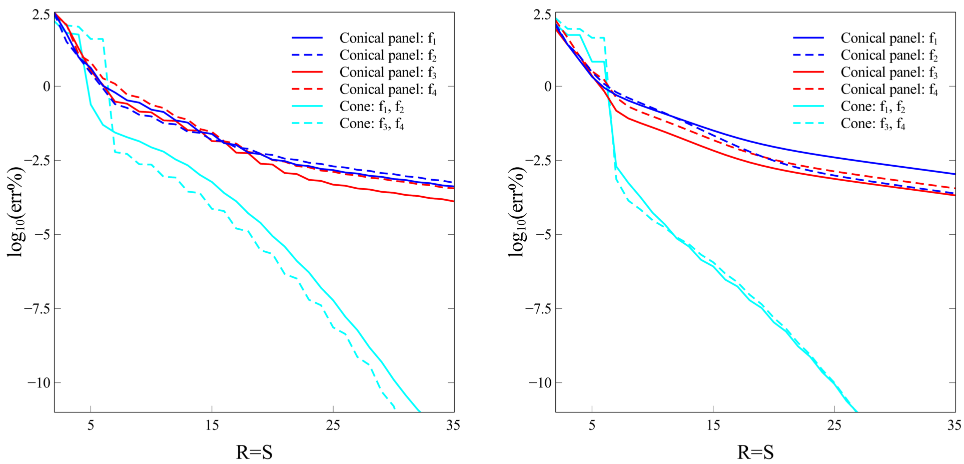

(a) (b)

Figure 3: Logarithmic error versus number of trial functions R=S for the first 4 frequencies for isotropic conical shells (a=2000 mm, R_i=500 mm, h=100 mm, α=40°) with different boundary conditions: (a) FFCF (panels, θ=120°), FC (cones), (b) FFss (panels, θ=120°), ss (cones).

	Cylindrical panel						Conical panel					
	FFCF			FFss			FFCF			FFss		
	Ritz	GDQ [39]	Abaqus	Ritz	GDQ [39]	Abaqus	Ritz	GDQ [39]	Abaqus	Ritz	GDQ [39]	Abaqus
	20×20			22×22			23×23			20×20		
f_1 (Hz)	58.28	58.32	58.83	76.14	76.18	77.11	76.77	76.80	77.04	90.91	90.92	91.40
f_2 (Hz)	90.61	90.62	91.76	188.04	188.14	187.80	106.54	106.53	106.82	170.07	170.04	170.99
f_3 (Hz)	146.27	146.35	144.55	232.35	232.26	233.24	152.13	152.17	152.61	232.30	232.33	233.27
f_4 (Hz)	230.76	230.72	232.34	285.34	285.37	285.34	187.12	187.12	188.01	272.37	272.43	272.51
f_5 (Hz)	263.70	263.63	265.83	428.66	428.84	426.00	248.59	248.57	249.60	312.83	312.85	314.53
f_6 (Hz)	278.69	278.56	278.71	467.61	467.63	467.81	262.03	262.12	261.75	324.54	324.61	328.27
f_7 (Hz)	339.26	339.43	339.07	537.11	537.52	537.67	308.46	308.50	308.65	374.65	374.71	374.94
f_8 (Hz)	430.65	430.81	427.41	573.67	573.73	573.17	345.86	345.90	347.44	411.08	411.13	414.21
CPU time (s)	≈ 1.1	/	≈ 13	≈ 1.3	/	≈ 13	≈ 1.5	/	≈ 11	≈ 1.1	/	≈ 11

Table 1: Dimensional frequencies f_i for isotropic cylindrical (R_i=1000 mm) and conical (R_i=500 mm, α=40°) panels – a=2000 mm, h=100 mm, θ=120°.

employed. Note, Ritz predictions are sometimes larger, sometimes smaller than the GDQ ones, although the percent differences are always well below 0.1%. When comparing with Abaqus, the differences are still very small, with the maximum discrepancies of 1%, approximately. The CPU times for a single run are reported for each configuration. The results refer to the time on a computer with Intel(R) Core(TM) i7-6700 processor with 32 GB of RAM. Rather than the time itself, it is interesting to observe the ratio between the time required by the Abaqus simulations and the Ritz ones. The speedup obtained with Ritz is noticeable and additional advantage is obtained due to the reduced time required for the modeling phase.

The second set of results refers to the case of closed shells. The results are presented in Table 2 for cylinders and cones.

The first ten frequencies are reported. Indeed, owing to the axisymmetry of the problem, all the eigenvalues are double. The only exception regards the cylinder under FC conditions, exhibiting the 9^{th} and 10^{th} frequencies different from one another. The same behaviour is observed in the reference results, where the predicted frequencies are still in excellent agreement with the DQM and Abaqus ones. Note, the presence of a free edge does not alter the quality of the results despite the challenges associated with the free edge natural conditions. Looking at Table 2, it is interesting to observe that, consistently with the results of Figures 2 and 3, a smaller number of Ritz functions is needed to achieve convergence with respect to the open shell case. A number of 9 and 14 functions suffices for the boundary conditions clamped-free and simply-supported, respectively. This behaviour is explained by observing that the periodicity condition in closed-shells is inherently satisfied by the trial functions adopted. Thus, the method is required to approximate the natural conditions at the top and bottom, only. On the contrary, the force conditions along four sides have to be approximated during the convergence process for the open panels, resulting in a stronger requirement over the number of functions to be used. This behaviour is opposite to the DQM case, as outlined in Ref. [39]. Indeed, the DQM method requires periodicity conditions to be enforced, resulting in slower convergence for closed shells with respect to open ones. The computational times in Table 2 provide clear evidence of the effectiveness of the present method and the drastic speedup with respect to finite element simulations. It is worth mentioning that refined finite element meshes are needed for the cylinders investigated here in order to guarantee the convergence of the fifth and sixth frequencies. This consideration explains the even larger computational saving achieved for cylinders.

Example 2: cross-ply conical shells

To address the case of shells made of composite material, the example presented by Wu and Lee [64] is discussed. Specifically an antisymmetrically, cross-ply layered conical shell is studied. The geometry is defined by a semi-vertex angle α=30°, bottom radius R_e=1000 mm and cone length a=500 mm. Different ratios h/R_e are investigated to illustrate the case of thin up to moderately thick shells. The orthotropic material is characterized by the nondimensional properties E_1/E_2=15, G_{12}/E_2=0.5, G_{13}/E_2=G_{23}/E_2=0.3846, and ν_{12}=0.25.

The results are summarized in Table 3 in terms of the nondimensional parameter $\Omega_i = \omega_i R_e \sqrt{\rho h/A_{11}}$ for

	Cylinder						Cone					
	FC			ss			FC			ss		
	Ritz	GDQ [39]	Abaqus	Ritz	GDQ [39]	Abaqus	Ritz	GDQ [39]	Abaqus	Ritz	GDQ [39]	Abaqus
	14×14			9×9			14×14			9×9		
f_1,f_2 (Hz)	146.11	146.17	144.81	330.96	331.15	329.45	200.63	200.69	200.57	208.65	208.69	207.93
f_3,f_4 (Hz)	210.20	210.32	208.84	348.31	348.46	347.30	221.60	221.65	221.41	222.66	222.70	221.99
f_5,f_6 (Hz)	242.56	242.55	242.44	440.57	440.86	439.32	274.74	274.77	274.61	250.31	250.33	249.62
f_7,f_8 (Hz)	366.39	366.58	365.72	508.02	508.07	507.76	308.27	308.30	308.29	318.09	318.11	317.70
f_9 (Hz)	402.24	401.91	402.53	595.99	596.25	593.21	341.08	341.16	340.24	318.62	318.66	318.07
f_{10} (Hz)	412.23	412.36	408.16	595.99	596.25	593.21	341.08	341.16	340.26	318.62	318.66	318.08
CPU time (s)	$\approx$ 0.7	/	$\approx$ 35	$\approx$ 0.6	/	$\approx$ 37	$\approx$ 0.7	/	$\approx$ 21	$\approx$ 0.6	/	$\approx$ 23

Table 2: Dimensional frequencies f_i for isotropic cylinders (R_i=1000 mm) and cones (R_i=500 mm, α=40°) panels – a=2000 mm, h=100 mm.

different lay-ups and boundary conditions. The comparison is illustrated against results from the literature for FSDT [64] and CLT [65] theories. In both reference papers, computations are performed via GDQ method.

		[0/90]				$[0/90]_{10}$			
Boundary conditions: ss	h/R_e:	0.01	0.04	0.07	0.10	0.01	0.04	0.07	0.10
DQ (FSDT) [64]		0.1759	0.2520	0.3061	0.3484	0.1958	0.2882	0.3544	0.3940
Ritz (FSDT)		0.1759	0.2520	0.3061	0.3484	0.1958	0.2882	0.3544	0.3940
GDQ (CLT) [65]		0.1799	0.2620	0.3277	0.3863	0.1976	0.2987	0.3873	0.4502
Ritz (CLT)		0.1770	0.2575	0.3216	0.3793	0.1976	0.2988	0.3870	0.4496
Boundary conditions: CC	h/R_e:	0.01	0.04	0.07	0.10	0.01	0.04	0.07	0.10
DQ (FSDT) [64]		0.3045	0.6986	0.9476	1.0831	0.3720	0.8836	1.1025	1.2020
Ritz (FSDT)		0.2966	0.6986	0.9476	1.0831	0.3720	0.8836	1.1025	1.2020
GDQ (CLT) [65]		0.2986	0.7752	1.2344	1.5737	0.3771	1.0992	1.5730	1.5737
Ritz (CLT)		0.2982	0.7685	1.2144	1.5731	0.3769	1.0941	1.5727	1.5731

Table 3: Nondimensional frequencies $\Omega_i = \omega_i R_e \sqrt{\rho h/A_{11}}$ for antisymmetrically layered composite cones (R_e=1000 mm, a=500 mm, α=30°).

As seen, the FSDT results are identical with those reported in Ref. [64], the only exception being the CC shell with a 2-ply lay-up and h/R_e=0.01. In this case, the Ritz solution provides a smaller frequency parameter. This slight discrepancy is likely due to a non-converged result in the reference work. The excellent results for all the cases of Table 3 give evidence of the ability of the approach to appropriately handling also the case of orthotropic materials. The results are reported also in the case of the Ritz implementation based on CLT, and the comparison is shown against the formulation proposed by Shu [65]. Also in this case, the Ritz results are in good agreement with the reference ones. Slightly smaller frequency parameters, ascribed to the improved spatial representation of the Ritz models, are observed. One can note the close agreement with FSDT ones for thin shells, i.e. h/R_e=0.01, and the increasingly larger differences as the shells get thicker.

Example 3: anisotropic cylindrical shells

An important feature in the development of a Ritz formulation regards the choice of a complete set of trial functions. The adoption of sets not respectful of this requirement is not uncommon in the literature, see Ref. [61] for further details, and may lead to erroneous results.

The example in this section aims at highlighting the importance of this aspect, which is often overlooked when dealing with anisotropic laminates. The test case is taken from Ref. [35], where composite cylinders with radius R=1000 mm, length a= 5000 mm and total thickness of 50 mm are studied. The material properties are given as E_1/E_2=25, G_{12}/E_2=G_{13}/E_2=0.5, G_{23}/E_2=0.2 and ν=0.25. Simply-supported boundary conditions SS are considered on both ends and two lay-ups are studied, [0/15/0] and [0/45/0]. The presence of the mid off-axis ply promotes membrane and bending anisotropy for both configuration. This, in turn, has a strong influence on the pattern of the modal shapes, as discussed next.

The results are presented in Table 4 in terms of the nondimensional frequency parameter $\Omega_i = \omega_i a^2/h\sqrt{\rho/E_{22}}$. Specifically, the results illustrate the predictions obtained using different sets of functions:

- E1: it refers to Eqs. (25)-(27), which is a full trigonometric expansion along the circumferential direction and Legendre polynomials in the axial direction. E1 is a complete set, and it is the one implemented in the present approach

- E2: it the trigonometric Navier-like expansion, where the displacements are expanded based on the well-known Navier solution. This expansion is not complete, nor in the circumferential, nor in the axial direction. For special cases, such as isotropic panels and cross-ply laminates, this expansion leads to the exact solution of the problem, as the contributions of the missing terms of the expansion is identically null.

- E3: it the expansion proposed in Ref. [64], where Navier-like expansion is adopted along the circumferential direction and Jacobi polynomials along the axial one. The expansion is complete along the axial direction, but incomplete along the circumferential one; this strategy is suitable only for those cases where a Navier solution exists.

Expansion type – lay-up [0/15/0]			Expansion type – lay-up [0/45/0]		
E1 - Full	E2 - Navier	E3 - [35]	E1 - Full	E2 - Navier	E3 - [35]
88.7502 (3,1)	92.7578 (3,1)	92.726 (3,1)	95.3350 (3,1)	101.4691 (3,1)	101.430 (3,1)
110.0765 (2,1)	118.2269 (4,1)	/	120.3761 (2,1)	128.9752 (4,1)	/
117.1162 (4,1)	119.3493 (2,1)	119.339 (2,1)	127.8942 (4,1)	146.9784 (2,1)	146.966 (2,1)
174.4610 (5,1)	174.7493 (5,1)	/	191.2082 (5,1)	192.4726 (5,1)	/
177.2073 (4,2)	181.2878 (4,2)	/	194.8871 (4,2)	211.9171 (4,2)	/
184.3546 (3,2)	192.7116 (3,2)	192.650 (3,2)	205.9959 (3,2)	236.3420 (5,2)	/
187.3176 (1,1)	203.9013 (1,1)	203.900 (1,1)	210.4095 (1,1)	253.2568 (3,2)	253.192 (3,2)
211.0075 (5,2)	212.5777 (5,2)	/	231.4395 (5,2)	275.1280 (6,1)	/
238.0838 (2,2)	249.1046 (6,1)	/	269.9348 (2,2)	299.5041 (1,1)	299.499 (1,1)
248.9868 (6,1)	251.7480 (2,2)	251.729 (2,2)	272.2800 (6,1)	302.6407 (6,2)	/

Table 4: Nondimensional frequencies $\Omega_i = \omega_i a^2/h\sqrt{\rho/E_{22}}$ for SS composite cylinders (R_i=1000 mm, a=5000 mm, h=50 mm) with anisotropic lay-ups: comparison between different sets of functions (in the brackets: (m, n), with m number of waves along the circumferential direction and n number of halfwaves along the axial direction).

The results in Table 4 refer to two lay-ups for which a Navier solution cannot be found due to the presence of an off-axis ply. The frequency parameters in the table demonstrate the equivalence between E2 and E3 for the cylinders under investigation. Despite the adoption of different approximations along the axial directions, the two solutions converge to the same results – the discrepancies are very small and due to round-off errors. However, the comparison against the complete set E1 demonstrates relatively large errors, which are due to the uncompleteness of the basis E2 and E3. In particular, one can note that the adoption of the sets E2 and E3 leads to larger parameters Ω_i: the missing terms of the expansions act as an internal, fictitious constraint, that provides extra stiffness to the model. As seen from the table, the magnitude of the error depends on the degree of anisotropy and, in particular, it is larger for the configuration with the midply oriented at 45. From the modal shape perspective, the uncompleteness of the basis implies that any skewness of the deflected pattern cannot be captured, meaning that the cylinder is fictitiously forced to exhibit non-skew eigenvectors. The first three eigenmodes are reported in Figure 4 for the configuration with lay-up [0/45/0].

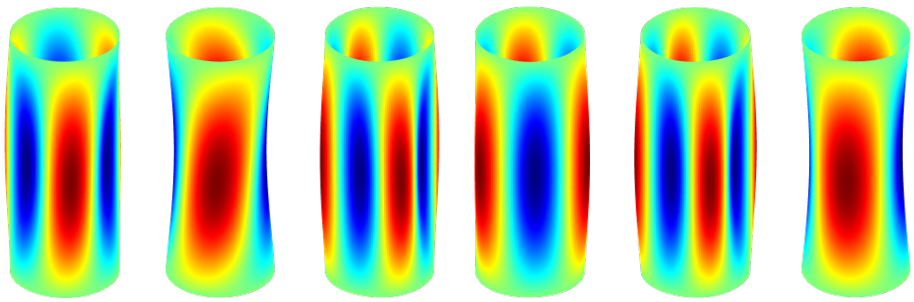

(a) Mode 1 (b) Mode 2 (c) Mode 3 (d) Mode 1 (e) Mode 2 (f) Mode 3

Figure 4: First three vibration modes for SS composite cylinder (R_i=1000 mm, a=5000 mm, h=50 mm) with lay-up [0/45/0] and using different sets of trial functions: (a)-(c) E1; (d)-(f) E2/E3.

The deflected shapes of Figures 4(a) and 4(c) refer to the trial functions E1/E2, while those of Figures 4(d) and 4(f) are obtained with the expansion E3. As seen, the erroneous use of incomplete sets does not allow the skewness of the pattern to be captured. For this specific case, one can also note the reversal between the second and the third modal shapes.

Example 4: FGM conical panels

To further extend the class of structures analyzed using the present formulation, a test case is proposed regarding the analysis of FGM conical panels. The materials are zirconia – E_c=151 GPa, ν_c=0.3 and ρ_c=3000 kg/m^3 – and aluminum – E_m=70 GPa, ν_m=0.3 and ρ_m=2707 kg/m^3 – whose power-law distribution to describe the volume fraction V_c along the thickness reads $V_c = \left(1/2 + z/h\right)^n$. The panel geometry is characterized by a=800 mm, R_i=200 and θ=120°. The thickness is equal to 1 mm and the shear factor is computed as $K_s = 5/(6 - (\nu_c V_c + \nu_m V_m))$, where V_c and V_m are the volume fractions of the ceramic and metal materials, respectively. Boundary conditions of type FFCF are considered. The results are reported in Table 5 in terms of the first four nondimensional parameters $\Omega_i = \omega_i a^2 \sqrt{\rho_c/(E_c h^2)}/2\pi$.

As seen, close agreement is achieved between the meshless method of Ref. [66] and the present Ritz implementation for all the six configurations obtained for different opening angles α and power-law parameters n. In all cases, the Ritz approach provides slightly larger predictions. As clear form the table, the Ritz frequencies

	n:	0.5				10			
α		Ω_1	Ω_2	Ω_3	Ω_4	Ω_1	Ω_2	Ω_3	Ω_4
15°	Meshless [66]	1.2486	2.0499	3.2488	3.5035	1.0404	1.7509	2.6914	2.9695
	Ritz (20×20)	1.2572	2.0565	3.2834	3.5400	1.0480	1.7562	2.7174	3.0005
	Ritz (30×30)	1.2570	2.0563	3.2831	3.5394	1.0478	1.7561	2.7172	3.0000
30°	Meshless [66]	1.5208	1.8121	2.9883	3.3348	1.2642	1.5449	2.5461	2.8337
	Ritz (20×20)	1.5291	1.8229	3.0351	3.4074	1.2717	1.5541	2.5869	2.8935
	Ritz (30×30)	1.5288	1.8225	3.0340	3.4059	1.2715	1.5538	2.5860	2.8924
45°	Meshless [66]	1.5119	1.6157	2.6675	3.0344	1.2614	1.3738	2.2671	2.5939
	Ritz (20×20)	1.5201	1.6294	2.7167	3.1212	1.2690	1.3856	2.3102	2.6664
	Ritz (30×30)	1.5196	1.6289	2.7155	3.1192	1.2687	1.3851	2.3092	2.6649

Table 5: Nondimensional frequencies $\Omega_i = \omega_i a^2 \sqrt{\rho_c/(E_c h^2)}/2\pi$ for FGM conical panels (FFCF, R_i=200 mm, a=800 mm, h=10 mm, θ=120°).

obtained with 20×20 functions are at convergence, as no further reduction is achieved by enriching the expansion up to 30×30 terms.

4.2 Stiffened shells

In this second part, the potential of the proposed implementation is illustrated by considering the case of shells with stiffeners directed along the longitudinal and the circumferential directions, namely stringers and rings. This kind of structures are widely used in the aerospace industry – fuselage structures, rockets and space launchers are few but examples.

Example 1: isotropic stringer- and ring-stiffened shells

A preliminary example regards the comparison against the well-known analytical solution for simply-supported stiffened cylinders, available under the assumptions of smeared technique [48], i.e. assuming that the effect of stiffeners and rings can be averaged over the whole structure. This assumption is particularly useful for deriving simplified design formulas and holds whenever the modal shape is of global type, i.e. with halfwaves encompassing several stringers.

The test case is of interest for validating the proposed Ritz method as the Navier solution of Ref. [48] provides an exact solution to the problem. The cylinder under investigation has length of 603 mm, radius equal to 243 mm and thickness 0.71 mm. An isotropic material is considered with E=72.4 GPa and Poisson's ratio of 0.3. Two stiffening types are considered: in one case the shell is stiffened by 60 equally spaced longitudinal stiffeners; in the other, 25 rings are introduced. In both cases, the stiffening elements are blade-shaped, with height of 7.67 mm and width of 2.44 mm. For consistency with the formulation of Ref. [48], the results are calculated by neglecting the rotatory and in-plane inertia contributions, although this latter can be shown to have not negligible effects on the vibrational response.

The results are presented in Figure 5, where the dimensional frequencies are reported for different against the number of circumferential full waves n. The curves are parametrized over the number of longitudinal halfwaves m and are presented for the case of internal and external stiffening – i.e. the stiffener eccentricity is negative or positive, respectively.

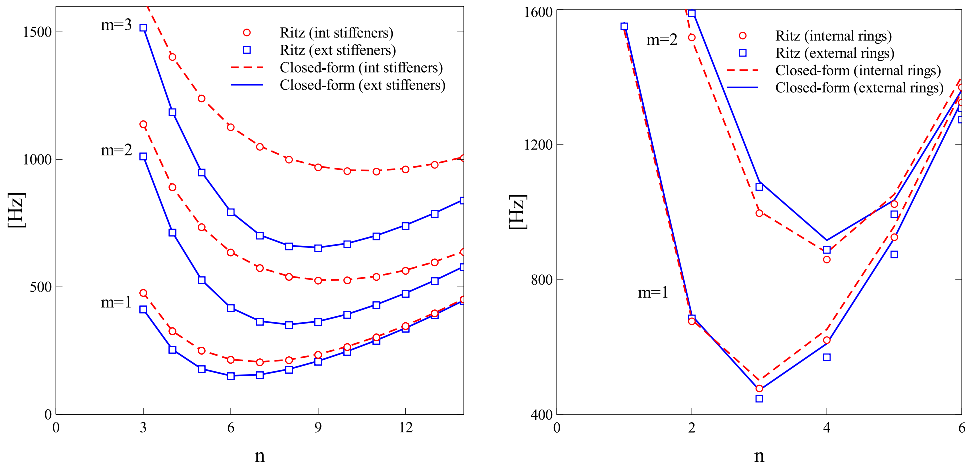

(a) (b)

Figure 5: Comparison between Ritz and Navier predictions for SS isotropic cylinders (R_i=243 mm, a=603 mm, h=0.71 mm) with equally spaced stringers and rings – Number of circumferential waves n against natural frequencies: (a) 60 stringers (h_s=7.67 mm, t_s=2.44 mm), (b) 25 rings (h_r=7.67 mm, t_r=2.44 mm).

The results for the stringer-stiffened cylinder are available in Figure 5(a), where the Ritz solution is found to be in close agreement with the Navier solution, both in terms of frequencies and modal shapes. The frequencies obtained for the ring-stiffened shell are reported in Figure 5(b): the agreement is still satisfactory, although some discrepancies can be noted. In particular, these deviations were found to be due to the simplifying Donnell-type assumptions employed in Ref. [48]. When the Ritz method is modified to account for Donnell assumptions, the error between Ritz and closed-form solution drops to zero. These results are not reported here for the sake of brevity.

An inherent restriction of smeared theories regards their inability to capture discreteness effects, which are generally not-negligible when the number of stiffening elements – stringers or rings – is not sufficiently large. In general, the threshold beyond which a smeared technique can be appropriate is problem-dependent, It is influenced by the shell geometry, as well as the stiffener section properties. To illustrate this effect, an assessment is reported in Figure 6, where the ratio $f_{\text{smear}}/f_{\text{disc}}$ is reported against the number of stringers. Here f_{smear} is the frequency obtained by smearing the stiffeners, while f_{disc} is the one obtained by treating the stiffeners as discrete elements.

The shells are characterized by ratios R/h=300, a/R=2.5 and thickness equal to 1 mm. The material is the same of the previous example, while boundary conditions are clamped-clamped and clamped-free.

In Figures 6(a) and 6(b), the nondimensional stiffener parameters are fixed. In particular, b_s is the distance between the equally space stringers, while $D = \dfrac{Eh^3}{12(1-\nu^2)}$ is the skin flexural stiffness. According to these nondimensional parameters, the smeared eigenvalues and eigenvectors do not change when the number of stiffeners is increased. On the contrary, they do modify when discrete effects are accounted for.

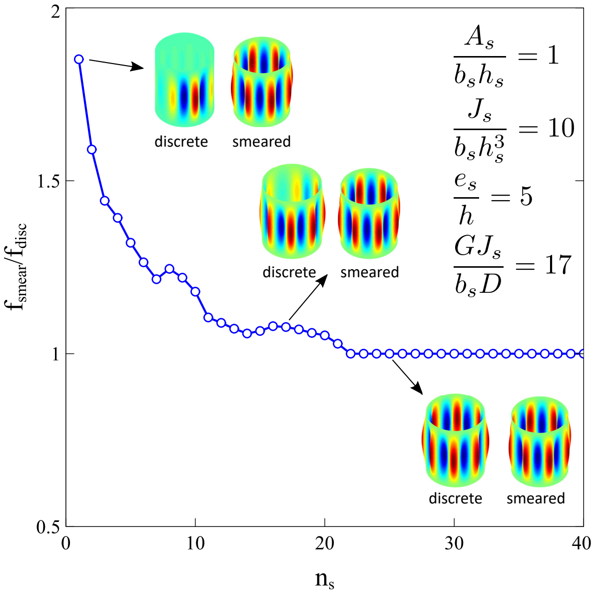

(a)

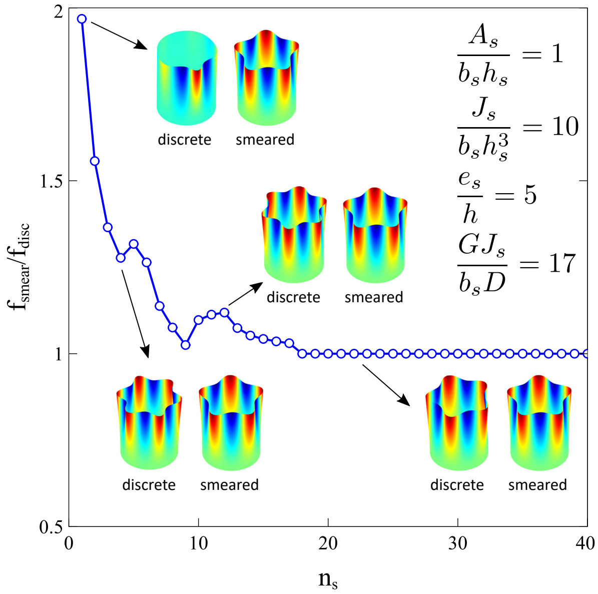

(b)

Figure 6: Effects of discreteness on free vibrations of isotropic cylinders (R/h=300, a/R=2.5) – Ratio between natural frequencies obtained by smearing the stiffeners and retaining their discreteness for increasing number of stringers n_s: (a) CC conditions, (b) CF conditions.

The two plots, relative to clamped-clamped and clamped-free boundary conditions, illustrate the high errors due to the smearing approach for a number of stringers below 20. In these cases, local effects cannot be neglected and discreteness must be considered. As expected, the smeared approach not only overpredicts the frequency value, but also provides an erroneous modal shape – exemplary comparisons between predicted eigenmodes are summarized in the plots. For values beyond 20, the two solutions converge to the same value, so the adoption of a smearing approach can be justified.

Smearing the stiffening elements provides just a slight advantage from a computational perspective. The number of unknowns is the same as in the case of discrete elements, while a relatively small number of integrals has to be computed. In spite of this small advantage, the range of employ is much more restricted and results can easily overpredict the frequencies whenever the modal shape is not purely of global type.

Example 2: anisotropic stringer- and ring-stiffened shells

This final example aims at providing reference results for relatively complex configurations. Specifically, a study is conducted for anisotropic cylindrical and conical panels with and without stiffening elements. The design is inspired by the isotropic panel analyzed in Ref. [47], which is translated here into a black metal counterpart. A sketch of the structures under investigation is reported in Figure 7, where the relevant dimensions and the position of the stiffening elements are reported as well. Both stringers and rings are placed on the outer side of the skin, corresponding to a positive value of the eccentricity measured from the skin midsurface. The shells are characterized by dimensions a=R_i=304.8 mm and opening angle θ=0.5 rad. For the conical shell, the semi-vertex angle is 45°.

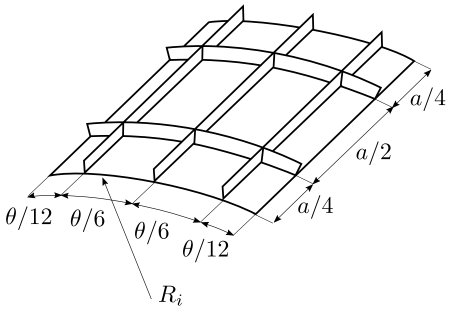

(a)

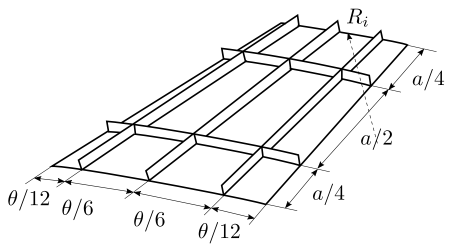

(b)

Figure 7: Stiffened panel configurations: (a) cylindrical panel, (b) conical panel.

A typical aerospace carbon/epoxy material is considered, IM7/8552, whose properties are taken as [67]: E_1= 150 GPa, E_2= 9000 MPa, G_{12}=G_{13}=5000 MPa, G_{23}=3500 MPa and ν_{12}=0.3. The density is equal to 1500 kg/m^3.

The skin is layered with the quasi-isotropic stacking sequence $[\pm 45/0/90]_{3\text{s}}$, where the ply thickness is 0.125 mm, leading to a total skin thickness of 3 mm. The section properties of stringers and rings are obtained by assuming rectangular sections of dimensions h_s=h_r=6.35 mm, t_s=8.2 mm, t_r=3.175 mm and the equivalent elastic properties of an homogeneous quasi-isotropic laminate, i.e. E_{iso}=57092 MPa and ν_{iso}=0.3092 (configuration St1). In addition, a second set of stiffening configuration is considered (configuration St2), where stringers and rings elastic properties are artificially increased by a factor of 10 while keeping all the other parameters unchanged. In doing so, the structures are more prone to display modes with local patterns, given the higher energy cost associated with deflections of global type. For generality, purposes, two sets of boundary conditions are considered, CFCF and CCCC.

The results are summarized in Table 6 where the first four nondimensional frequency parameters $\Omega_i = \omega_i R_e \sqrt{\rho h / A_{11}}$ are reported for the unstiffened and the stiffened cases.

One can note increasing frequency values starting from the unstiffened case and moving towards the stiffened

	Cylindrical panel			Conical panel (α=45°)		
	Unstiffened	Stiffened		Unstiffened	Stiffened	
BCs		St1	St2		St1	St2
CFCF	0.1164	0.1936	0.3373	0.1696	0.2857	0.5163
	0.1524	0.2032	0.3666	0.2112	0.3024	0.5321
	0.2664	0.4082	0.7270	0.3692	0.4804	0.8529
	0.3145	0.4620	0.8158	0.3987	0.6788	1.2013
CCCC	0.6914	0.7530	0.9421	0.6831	0.7446	1.0053
	0.8195	0.7785	1.1350	0.7325	0.8310	1.2792
	0.8436	0.9223	1.4341	0.8800	1.0341	1.6745
	0.8731	1.1473	1.5160	0.9529	1.2727	1.7991

Table 6: Nondimensional frequencies $\Omega_i = \omega_i R_e \sqrt{\rho h / A_{11}}$ for anisotropic panels (R_i=a=304.8 mm, h=3 mm, θ=0.5 rad) – Results for unstiffened and stiffened (configurations St1 and St2) under different boundary conditions.

configurations St1 and St2, the latter clearly associated with the highest frequency values owing to the improved stiffness properties. The first eigenmodes are summarized in Figures 8 and 9 for the cylindrical and conical panels, respectively. The results are obtained using 25×25 functions to guarantee accuracy in the prediction and can be useful for comparison purposes in future studies.

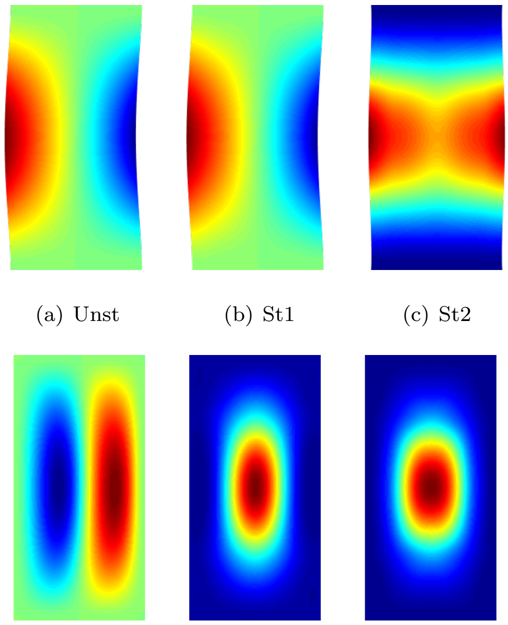

(a) Unst (b) St1 (c) St2

(d) Unst (e) St1 (f) St2

Figure 8: First vibration modes for ustiffened (Unst) and stiffened (configurations St1 and St2) anisotropic cylindrical panels (R_i=a=304.8 mm, h=3 mm, θ=0.5 rad) under different boundary conditions: (a)-(c) CFCF, (d)-(f) CCCC.

5 Conclusions

This work presented a formulation based on the Ritz method for the free vibration analysis of stiffened and unstiffened shells. The method is general enough to allow open and closed conical shells to be studied. Cylindrical ones are recovered as a special case. Any set of boundary conditions can be studied. No penalty terms are needed for this scope, which is advantageous in terms of numerical conditioning of the problem. The efficient implementation of the method relies on the analytical evaluation of the Ritz integrals not depending on the radius of curvature. These integrals are evaluated just once and then stored in memory. Any run just requires to load the corresponding values, overcoming a typical bottleneck of Ritz-based methods.

A set of test cases is presented revealing excellent agreement with the results from the literature. It is observed that convergence is generally faster for cylindrical shells with respect to conical ones. Furthermore, closed shells, if compared to open ones, tend to require less trial functions to achieve convergence. Worth of mention are the excellent results obtained even in the presence of free edges, despite the corresponding boundary conditions are satisfied in a weak-form sense.

The importance of employing a complete set of functions is demonstrated through exemplary test cases where anisotropy effects may lead to erroneous predictions if Navier-like expansions are used.

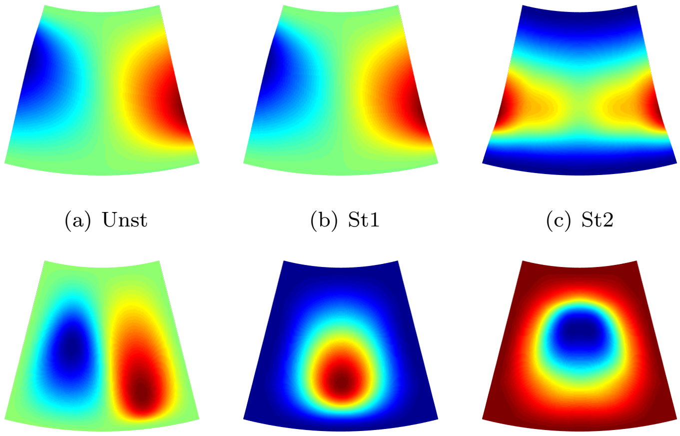

(a) Unst (b) St1 (c) St2

(d) Unst (e) St1 (f) St2

Figure 9: First vibration modes for ustiffened (Unst) and stiffened (configurations St1 and St2) anisotropic conical panels (R_i=a=304.8 mm, h=3 mm, θ=0.5 rad, α=45°) under different boundary conditions: (a)-(c) CFCF, (d)-(f) CCCC.

Stiffened configurations are handled in two ways, by smearing the stiffening elements or by accounting for their discreteness. Within a Ritz-based approach, the advantage of a smeared approach is mild. The computational effort is close to the one required by Ritz models accounting for discrete effects. On the contrary, practical restrictions exist on the modal shape, which is restricted to be of global type.

Overall, the proposed strategy can be a useful mean for investigating the vibrating behaviour of composite shells, with or without stiffeners and rings, in a fast yet accurate way. The modeling time is essentially null and the time for the analysis is of the order of a second. The adoption of a beam model does not allow local effects to be captured, but in most designs these effects are not of concern unless high frequency responses need to be investigated.

The class of configurations that can be analyzed with the proposed approach is relatively wide. However, future activity should be directed towards the extension of the method to handle typical features found in practical applications. More complex geometric patterns, including configurations with cutouts, modeling of manufacturing imperfections, as well as refined modeling of the stiffeners via 2D models will be the subjects of future investigations.

References

[1] B.L. Agarwal and L.H. Sobel. Weight comparisons of optimized stiffened, unstiffened, and sandwich cylindrical shells. *Journal of Aircraft*, 14(10):1000–1008, 1977.

[2] B. Budiansky. On the minimum weights of compression structures. *International Journal of Solids and*

Structures, 36(24):3677–3708, 1999.

[3] F. Tornabene and N. Fantuzzi. *Theory of Laminated Composite Doubly-Curved Shell Structures.* Società Editrice Esculapio, 2017.

[4] H. Kraus. *Thin Elastic Shells.* John Wiley & Sons, 1967.

[5] A.W. Leissa. Vibration of shells. Technical Report SP-288, NASA, 1973.

[6] E. Ventsel and T. Krauthammer. *Thin Plates and Shells: Theory, Analysis, and Applications.* Marcel Dekker, Inc., New York, 2001.

[7] J.N. Reddy. *Mechanics of Laminated Composite Plates and Shells: Theory and Analysis.* CRC Press, Boca Raton, 2004.

[8] M.S. Qatu. *Vibration of Laminated Shells and Plates.* Elsevier, 2004.

[9] M. Amabili. *Nonlinear Vibrations and Stability of Shells and Plates.* Cambridge University Press, 2008.

[10] L. Tong. Free vibration of composite laminated conical shells. *International Journal of Mechanical Sciences*, 35(1):47–61, 1993.

[11] L. Tong. Free vibration of laminated conical shells including transverse shear deformation. *International Journal of Solids and Structures*, 31(4):443–456, 1994.

[12] P.L. Gould. *Finite Element Analysis of Shells of Revolution.* Pitman Publishing, 1985.

[13] M.L. Bucalem and K.J. Bathe. Finite element analysis of shell structures. *Archives of Computational Methods in Engineering*, 4(1):3–61, 1997.

[14] M.F. Caliri, A.J.M. Ferreira, and V. Tita. A review on plate and shell theories for laminated and sandwich structures highlighting the Finite Element Method. *Composite Structures*, 156:63–77, 2016.

[15] E. Carrera, M. Cinefra, G. Li, and G.M. Kulikov. MITC9 shell finite elements with miscellaneous through-the-thickness functions for the analysis of laminated structures. *Composite Structures*, 154:360–373, 2016.

[16] M. Cinefra, E. Carrera, L. Della Croce, and C. Chinosi. Refined shell elements for the analysis of functionally graded structures. *Composite Structures*, 94(2):415–422, 2012.

[17] Y. Gu and L. Sun. Electroelastic analysis of two-dimensional ultrathin layered piezoelectric films by an advanced boundary element method. *International Journal for Numerical Methods in Engineering, 122(11):2653–2671, 2021.*

[18] Y. Gu and C. Zhang. Fracture analysis of ultra-thin coating/substrate structures with interface cracks. *International Journal of Solids and Structures*, 225:111074, 2021.

[19] K.M. Liew and C.W. Lim. Vibratory characteristics of cantilevered rectangular shallow shells of variable thickness. *AIAA Journal*, 32(2):387–396, 1994.

[20] K.M. Liew and C.W. Lim. Vibration of perforated doubly-curved shallow shells with rounded corners. *International Journal of Solids and Structures*, 3(11):1519–1536, 1994.

[21] C.W. Lim and K.M. Liew. Vibratory behaviour of shallow conical shells by a global Ritz formulation. *Engineering Structures*, 17(1):63–70, 1995.

[22] C.W. Lim and K.M. Liew. A higher order theory for vibration of shear deformable cylindrical shallow shells. *International Journal of Mechanical Sciences*, 37(3):277–295, 1995.

[23] K.M. Liew, T.Y. Ng, and X. Zhao. Free vibration analysis of conical shells via the element-free kp-Ritz method. *Journal of Sound and Vibration*, 281(3-5):627–645, 2005.

[24] F.M. Li, K. Kishimoto, and W.H. Huang. The calculations of natural frequencies and forced vibration responses of conical shell using the Rayleigh-Ritz method. *Mechanics Research Communications*, 36(5):595–602, 2009.

[25] G. Jin, T. Ye, and Z. Su. *Structural Vibration*. Engineering Structures, 2015.

[26] T. Ye, G. Jin, Z. Su, and X. Jia. A unified Chebyshev-Ritz formulation for vibration analysis of composite laminated deep open shells with arbitrary boundary conditions. *Archive of Applied Mechanics*, 84(4):441–471, 2014.

[27] K. Choe, K. Kim, and Q. Wang. Dynamic analysis of composite laminated doubly-curved revolution shell based on higher order shear deformation theory. *Composite Structures*, 225:111155, 2019.

[28] F. Pang, H. Li, X. Wang, X. Miao, and S. Li. A semi analytical method for the free vibration of doubly-curved shells of revolution. *Computers & Mathematics with Applications*, 75(9):3249–3268, 2018.

[29] B. Qin, R. Zhong, T. Wand, Q. Wang, Y. Xu, and Z. Hu. A unified Fourier series solution for vibration analysis of FG-CNTRC cylindrical, conical shells and annular plates with arbitrary boundary conditions. *Composite Structures*, 232:111549, 2020.

[30] L.E. Monterrubio. Free vibration of shallow shells using the Rayleigh-Ritz method and penalty parameters. *Proceedings of the Institution of Mechanical Engineers, Part C: Journal of Mechanical Engineering Science*, 223(10):2263–2272, 2009.

[31] R. Vescovini and C. Bisagni. Semi-analytical buckling analysis of omega stiffened panels under multi-axial loads. *Composite Structures*, 120:285–299, 2015.

[32] S.G.P Castro, C. Mittelstedt, F.A.C. Monteiro, M.A. Arbelo, G. Ziegmann, and R. Degenhardt. Linear buckling predictions of unstiffened laminated composite cylinders and cones under various loading and boundary conditions using semi-analytical models. *Composite Structures*, 118:303–315, 2014.

[33] S.G.P Castro, C. Mittelstedt, F.A.C. Monteiro, M.A. Arbelo, R. Degenhardt, and G. Ziegmann. A semi-analytical approach for linear and non-linear analysis of unstiffened laminated composite cylinders and cones under axial, torsion and pressure loads. *Thin-Walled Structures*, 90:61–73, 2015.

[34] H. Li, F. Panf, Q. Gong, and Y. Teng. Free vibration analysis of axisymmetric functionally graded doubly-curved shells with un-uniform thickness distribution based on Ritz method. *Composite Structures*, 225:111145, 2019.

[35] H. Li, F. Pang, X. Miao, S. Gao, and F. Liu. A semi analytical method for free vibration analysis of composite laminated cylindrical and spherical shells with complex boundary conditions. *Thin-Walled Structures*, 136:200–220, 2019.

[36] Y. Kiani, R. Dimitri, and F. Tornabene. Free vibration study of composite conical panels reinforced with FG-CNTs. *Engineering Structures*, 172:472–482, 2018.

[37] A.H. Sofiyev. The vibration and stability behavior of freely supported FGM conical shells subjected to external pressure. *Composite Structures*, 89(3):356–366, 2009.

[38] A.H. Sofiyev and E. Schnack. The stability of functionally graded cylindrical shells under linearly increasing dynamic torsional loading. *Engineering Structures*, 26(10):1321–1331, 2004.

[39] F. Tornabene, E. Viola, and D.J. Inman. 2-D differential quadrature solution for vibration analysis of functionally graded conical, cylindrical shell and annular plate structures. *Journal of Sound and Vibration*, 328(3):259–290, 2009.

[40] J.C. Monge and J.L. Mantari. 3D elasticity numerical solution for the static behavior of FGM shells. *Engineering Structures*, 208:110159, 2020.

[41] A.H. Sofiyev. Review of research on the vibration and buckling of the FGM conical shells. *Composite Structures*, 211:301–317, 2019.

[42] A.M.J. Al-Najafi and G.B. Warburton. ree vibration of ring-stiffened cylindrical shells. *Journal of Sound and Vibration*, 13(1):9–25, 1970.

[43] A. Mukherjee and M. Mukhopadhyay. Finite element free vibration analysis of stiffened plates. *The Aeronautical Journal*, 90(897):267–273, 1986.

[44] B.A.J. Mustafa and R. Ali. Prediction of natural frequency of vibration of stiffened cylindrical shells and orthogonally stiffened curved panels. *Journal of Sound Vibration*, 113(2):317–327, 1987.

[45] J. Jiang and M.D. Olson. Vibration analysis of orthogonally stiffened cylindrical shells using super finite elements. *Journal of Sound and Vibration*, 173(1):73–83, 1994.

[46] G. Sinha and M. Mukhopadhyay. Finite element free vibration analysis of stiffened shells. *Journal of Sound Vibration*, 171(4):529–548, 1994.

[47] A. Samanta and M. Mukhopadhyay. Free vibration analysis of stiffened shells by the finite element technique. *European Journal of Mechanics-A/solids*, 23(1):159–179, 2004.

[48] M.M. Mikulas and J. McElman. On free vibrations of eccentrically stiffened cylindrical shells and flat plates. TN D-3010, NASA, 1965.

[49] R. Ruotolo. A comparison of some thin shell theories used for the dynamic analysis of stiffened cylinders. *Journal of Sound and Vibration*, 243(5):847–860, 2001.

[50] M. Hemmatnezhad, G.H. Rahimi, and R. Ansari. On the free vibrations of grid-stiffened composite cylindrical shells. *Acta Mechanica*, 225(2):609–623, 2014.

[51] M. Hemmatnezhad, G.H. Rahimi, M. Tajik, and F. Pellicano. Experimental, numerical and analytical investigation of free vibrational behavior of gfrp-stiffened composite cylindrical shells. *Composite Structures*, 120:509–518, 2015.

[52] M. Zarei, G.H. Rahimi, and M. Hemmatnezhad. Free vibrational characteristics of grid-stiffened truncated composite conical shells. *Aerospace Science and Technology*, 99:105717, 2020.

[53] M. Zarei, G.H. Rahimi, and M. Hemmatnezhad. On the free vibrations of joined grid-stiffened composite conical-cylindrical shells. *Thin-Walled Structures*, 161:107465, 2021.

[54] M.P. Nemeth. A treatise on equivalent-plate stiffnesses for stiffened laminated-composite plates and plate-like lattices. Technical Report TP-2011-216882, NASA, 2011.

[55] D. Egle and J.L. Sewall. An analysis of free vibration of orthogonally stiffened cylindrical shells with stiffeners treated as discrete elements. *AIAA Journal*, 6(3):518–526, 1968.

[56] B.A.J. Mustafa and R. Ali. An energy method for free vibration analysis of stiffened circular cylindrical shells. *Computers & Structures*, 32(2):355–363, 1989.

[57] S.S. Rao and E.S. Reddy. Optimum design of stiffened conical shells with natural frequency constraints. *Computers & Structures*, 14(1–2):103–110, 1981.

[58] Z. Mecitoğlu. Vibration characteristics of a stiffened conical shell. *Journal of Sound and Vibration*, 197(2):191–206, 1996.

[59] A.A. Jafari and M. Bagheri. Free vibration of non-uniformly ring stiffened cylindrical shells using analytical, experimental and numerical methods. *Thin-Walled Structures*, 44(1):82–90, 2006.

[60] M. Talebitooti, M. Ghayour, S. Ziaei-Rad, and R. Talebitooti. Free vibrations of rotating composite conical shells with stringer and ring stiffeners. *Archive of Applied Mechanics*, 80(3):201–215, 2010.

[61] R. Vescovini, L. Dozio, M. D'Ottavio, and O. Polit. On the application of the Ritz method to free vibration and buckling analysis of highly anisotropic plates. *Composite Structures*, 192:460–474, 2018.

[62] J.N. Reddy. *Energy Principles and Variational Methods in Applied Mechanics*. John Wiley and Sons, New York, USA, 1984.

[63] H. Baruh and S.S.K. Tadikonda. Another look at admissible functions. *Journal of Sound and Vibration*, 132(1):73–87, 1989.

[64] C.P. Wu and C.Y. Lee. Differential quadrature solution for the free vibration analysis of laminated conical shells with variable stiffness. *International Journal of Mechanical Sciences*, 43(8):1853–1869, 2001.

[65] C. Shu. Free vibration analysis of composite laminated conical shells by generalized differential quadrature. *Journal of Sound and Vibration*, 194(4):587–604, 1996.

[66] X. Zhao and K.M. Liew. Free vibration analysis of functionally graded conical shell panels by a meshless method. *Composite Structures*, 93(2):649–664, 2011.

[67] C. Bisagni, R. Vescovini, and C.G. Dávila. Single-stringer compression specimen for the assessment of damage tolerance of postbuckled structures. *Journal of Aircraft*, 48(2):495–502, 2011.